Howard Hughes Medical Institute

Published as: *Nat Neurosci*. 2016 February ; 19(2): 308–315.

Thalamus provides layer 4 of primary visual cortex with orientation- and direction-tuned inputs

Wenzhi Sun[1], **Zhongchao Tan**[1], **Brett D. Mensh**[1], and **Na Ji**[1,*]

[1]Janelia Research Campus, Howard Hughes Medical Institute, Ashburn, VA 20147, USA

Abstract

Understanding the functions of a brain region requires knowing the neural representations of its myriad inputs, local neurons, and outputs. Primary visual cortex (V1) has long been thought to compute visual orientation from untuned thalamic inputs, but very few thalamic inputs have been measured in any mammal. We determined the response properties of ~28,000 thalamic boutons and ~4,000 cortical neurons in layers 1–5 of awake mouse V1. With adaptive optics allowing accurate measurement of bouton activity deep in cortex, we found that around half of the boutons in the main thalamorecipient L4 carry orientation-tuned information, and their orientation/direction biases are also dominant in the L4 neuron population, suggesting that these neurons may inherit their selectivity from tuned thalamic inputs. Cortical neurons in all layers exhibited sharper tuning than thalamic boutons and a greater diversity of preferred orientations. Our results provide data-rich constraints for refining mechanistic models of cortical computation.

In the conventional pathway of mammalian early vision, information from the retina is conveyed by the dorsal lateral geniculate nucleus (dLGN) of the thalamus to L4 of primary visual cortex (V1) and, after computations in the cortical circuit, is communicated to the rest of the brain[1] (i.e., mainly dLGN → L4 → L2/3 → L5 →). Since the discovery of orientation selectivity in V1 neurons[2], how the mammalian nervous system computes the orientation of visual stimuli has been a flagship question in neuroscience.

Providing the principal thalamic inputs to V1 (Supplementary Fig. 1)[3], dLGN has long been thought to convey only untuned inputs to cortex. Orientation selectivity is therefore considered a feature computed in cortex, beginning at the first stage of thalamocortical interaction[4–6]. In the classical feedforward model of Hubel and Wiesel[7], cortical orientation selectivity is generated by the convergence of untuned dLGN inputs with offset receptive fields onto a L4 simple cell. Although such an arrangement has not been directly observed, existing experimental evidence is consistent with its basic premise that thalamic inputs to the main thalamorecipient L4 lack orientation tuning[8].

*Correspondence to: ; Email: jin@janelia.hhmi.org

Author Contributions N. J. initiated and oversaw the project, W. S. and N. J. designed the experiments, Z. T. collected calcium imaging data on L4 neurons, W. S. collected all other data. All authors contributed to data analysis and presentation. W. S., B. D. M., and N. J. wrote the paper.

In mouse, some dLGN neurons encode information about the orientation and/or direction of moving stimuli[9–12]. This is not surprising, given the prevalence of direction-selective ganglion cells in mouse retina[13]. But do the tuned thalamic neurons send their axons to the main thalamo-recipient L4 of V1, where they may contribute to the cortical representation of orientation? A recent report[14] suggests that mouse dLGN provides tuned inputs to L1, but not L4, upholding the longstanding belief that orientation and direction selectivity in the bulk of V1 neurons arise predominantly from the convergence of untuned thalamic inputs[15].

In this study, we used the calcium indicator GCaMP6s[16] and *in vivo* functional calcium imaging to measure the orientation and motion direction tuning properties of ~28,000 thalamic boutons, as well as ~1,200 L4, ~1,300 L2/3, and ~1,600 L5 neurons in V1 of head-fixed awake mice. We show that large proportions of thalamic inputs to cortical layers 1–4 are tuned, and that on the population level, have strong biases towards specific orientations and directions. These biases overlap with the biases observed in V1's L4 population, although cortical neurons have overall sharper tuning and a greater diversity of preferred orientations than thalamic boutons. Our results contradict the longstanding belief that thalamus only provides untuned representations to L4 of V1, and imply that at least some of the orientation and direction tuning observed in V1 is inherited from thalamic inputs that are individually tuned for orientation and motion direction.

RESULTS

In vivo imaging of thalamic boutons in V1 of awake mice

To characterize the orientation tuning properties of thalamocortical afferents in V1, we transfected dLGN neurons in wild-type mice with the calcium indicator GCaMP6s and measured changes in two-photon fluorescence of the GCaMP6s$^+$ axons in V1 when visual stimuli were presented to the contralateral eye (Fig. 1a,b). Because thalamic axons ramify not only in L4 but also in the supragranular layers (L1 and L2/3)[17] (Supplementary Fig. 2, Fig. 1c), we imaged axons ranging from 0 to 400 μm below the pia of V1 (Fig. 1d–f). We habituated awake mice to head fixation to minimize movement during imaging; residual motion was corrected by an iterative cross-correlation-based registration algorithm[18] (Methods, Supplementary Fig. 3). During presentation of square gratings drifting in one of 8 directions (presented in a pseudorandom sequence), individual micron-sized varicosities along the axonal arborizations exhibited local visually evoked increases in fluorescence (**Supplementary Videos 1, 2**), thus were putative presynaptic boutons[19–21]. Of 34,120 boutons (21 mice) chosen for analysis, ~90% were determined to be from distinct cells through correlation coefficient analysis[20] (Supplementary Fig. 4). We classified the visually responsive boutons (those with $\Delta F/F > 10\%$) according to their orientation selectivity to drifting-grating stimuli (Fig. 1g–i). For each bouton that had a significant response-anisotropy by ANOVA ($P < 0.05$), we calculated its orientation tuning curve from its averaged calcium transient ($\Delta F/F$, bottom six $\Delta F/F$ traces in Fig. 1j–l) across 10 sets of trials (Fig. 1m–o). Only boutons whose tuning curves were well-fit by a bimodal Gaussian function[22] (Methods) were considered orientation selective (OS).

Tuning curves of boutons are sensitive to the optical aberrations caused by the differences in refractive indices between the immersion medium (e.g., water) and the cranial window

and/or brain tissue[23] (Fig. 2a). These refractive-index differences distort the wavefront of the laser used for two-photon excitation and leads to the degradation of image resolution by enlarged focal volume and the loss of signal via reduced focal intensity (Fig. 2b). The consequent deterioration of image quality is particularly severe for smaller structures (e.g., boutons) and larger aberration (e.g. thick cranial window). With a 340-μm thick cranial window, 70% of all boutons (n=1,056, 3 mice) appeared to be non-responsive to visual stimuli and only 7% satisfied OS criteria. With a thinner cranial window of 170-μm thickness, we found 31% OS boutons (of total n=1,302, 5 mice), still substantially fewer than 48% OS boutons as determined when the same boutons (n=1,477, 5 mice) were imaged after aberration correction by adaptive optics (AO) (Fig. 2c). These discrepancies can be understood by comparing the calcium transients of individual boutons: aberration reduces calcium transient magnitude from boutons of interest (red circles in Fig. 2d) but increases contamination from other active boutons within the enlarged focus, therefore can artifactually reduce tuning and cause shifts of preferred orientations[24, 25] (Fig. 2e). These artifacts were also observed on the population level, as indicated by the distributions of global orientation-selectivity index (Fig. 2f, without AO, median=0.21; with AO, median=0.26; see below for definition) and preferred orientation (Fig. 2g) (same 170-μm window data as in Fig. 2c). Therefore, in order to accurately characterize the response properties of the thalamic boutons, we used adaptive optics to remove cranial-window aberrations for all experiments.

Across all depths, we observed an approximately equal mix of non-orientation-selective (e.g., top three $\Delta F/F$ traces in Fig. 1j–l) (48%, n=13,424, 21 mice) and orientation-selective (OS, bottom six $\Delta F/F$ traces in Fig. 1j–l, with their corresponding tuning curves shown in Fig. 1m–o) (52%, n=14,478, 21 mice) boutons. The observation that both the supragranular and granular afferents carry orientation-tuned information contradicts the prevailing view that L4 geniculate inputs are not orientation-tuned.

In vivo imaging of cortical neurons in V1 of awake mice

To delineate the progression of neural representations of orientation and direction within V1, we followed the canonical circuit L4 → L2/3 → L5 and selectively labelled the excitatory neurons in L4 (*Scnn1a*-Tg3-Cre[26]), L2/3 (*Thy1*-GCaMP6 GP4.3[27]), and L5 (*Rbp4*-Cre[21]) of V1 with GCaMP6s. We characterized the tuning properties of these neurons by measuring their somatic calcium responses to drifting gratings in head-fixed awake mice (Fig. 3). Using the same criteria as for boutons, we found that 83% of visually responsive L4 (n=1,239, 3 mice), 83% of responsive L2/3 (n=1,279, 6 mice), and 60% of responsive L5 (n=1,637, 5 mice) neurons are OS.

Orientation tuning of thalamic boutons in V1

We separately characterized the orientation tuning properties of thalamic boutons in L1 (depth below pia: 0–100 μm, n=11,697, 19 mice, 50% OS), L2/3 (150–250 μm, n=6,076, 17 mice, 47% OS), and L4 (300–400 μm, n=10,129, 14 mice, 55% OS) of V1 (Fig. 4a–o, Methods). Although the full range of preferred orientation angles were observed, tuned inputs to L1 through L4 were strongly biased toward the vertical orientation. In the more superficial laminae, especially L1, we also observed a sizable fraction of boutons preferring

the horizontal orientation (Fig. 4a–c). This pattern of anisotropy is consistent with the view that the orientation selectivity in dLGN neurons originates from dLGN-projecting direction-selective retinal ganglion cells[12], which also prefer the cardinal directions[13].

We quantified orientation selectivity of each bouton two ways in order to enhance inferential robustness when comparing across populations. The global orientation-selectivity index (gOSI), defined as $\frac{|\sum_k R(\theta_k)e^{i2\theta_k}|}{\sum_k R(\theta_k)}$ with $R(\theta)$ being the measured response at orientation θ[28], yielded median values of 0.25–0.27 for OS boutons (open-bar histograms in Fig. 4d–f). As expected, for visually responsive boutons that had been classified as non-selective (by the method described above), gOSIs were lower (medians 0.12–0.13, gray-bar histograms in Fig. 4d–f). Another orientation-selectivity index (OSI), defined as $\frac{R_{\mathrm{pref}} - R_{\mathrm{ortho}}}{R_{\mathrm{pref}}+R_{\mathrm{ortho}}}$ with R_{pref} and R_{ortho} being the responses at the preferred and orthogonal orientations, respectively, yielded median values of 0.56 (Fig. 4g–i) across the OS bouton population in all 3 depth strata. Another measure of tuning-curve sharpness, full-width-at-half-maximum (FWHM), had medians of ~70° for axons in L1 and L2/3, and ~82° for axons in L4 (Fig. 4j–l).

Direction tuning of thalamic boutons in V1

Some of the orientation-tuned boutons also showed differential responses to the two motion directions for drifting gratings of their preferred orientation (e.g., bottom three $\Delta F/F$ traces in Fig. 1j–l). To characterize the preferred motion direction of the thalamic inputs, we calculated the direction-selectivity index (DSI) for each OS bouton defined as $\frac{R_{\mathrm{pref}} - R_{\mathrm{oppo}}}{R_{\mathrm{pref}}+R_{\mathrm{oppo}}}$, where R_{pref} and R_{oppo} are the responses at the preferred motion direction and its opposite, respectively. Using this index, we classified the OS boutons into two populations: those with DSI < 0.5 were defined as axis-selective (AS, equivalent to "orientation-selective but not motion-direction selective") (e.g., Fig. 5a), whereas those with DSI > 0.5 (3× or stronger response to gratings drifting in the preferred direction than its opposite) were defined as direction-selective (DS) (e.g., Fig. 5b). With this criterion, across all depths, around half of the orientation-tuned thalamic inputs were AS and half were DS (median DSIs of boutons were 0.46–0.49 across cortical depths, Fig. 4m–o).

For both AS and DS boutons, their respective gOSI and OSI distributions were similar across depths (Fig. 5c–h). DS boutons had a larger proportion of units with very broad orientation-tuning (FWHM > 120°) (Fig. 5i–k), yet high direction-selectivity. We found that the population of AS inputs to L1 selects for both horizontally- and vertically-moving gratings (Fig. 5l), but with increasing projection depth, the vertical motion bias fades away – AS inputs at L4 overwhelmingly prefer near-horizontal movement (Fig. 5m,n). The DS inputs across L1 through L4 strongly and consistently prefer the posterior-to-anterior motion direction (Fig. 5o–q). This direction bias can even be seen from the population responses of thalamic boutons, calculated by averaging the calcium transients of all responsive boutons, with their mean vectors aligned along the posterior-to-anterior direction at all layers (Supplementary Fig. 5).

Orientation and direction tuning of L4 neurons in V1

Geniculate afferents densely form synapses with neurons in the principal thalamorecipient L4. We therefore asked whether L4 neurons share the orientation and direction biases of the thalamic inputs. Compared to their thalamic inputs, neurons in L4 are more orientation-selective (median gOSI = 0.56, median OSI = 0.78, Fig. 4q,r) with correspondingly narrower tuning widths (median FWHM = 33.6°, Fig. 4s)[9]. The near-vertical orientations that dominate the preferred-orientation distribution of the thalamic inputs are also the most prominent orientation preference of OS L4 neurons (Fig. 4p).

Furthermore, after dividing the OS L4 neurons into AS (n=571, 46% of all visually responsive neurons) and DS (n=452, 37% of all visually responsive neurons) populations using the same DSI criterion (Fig. 4t, 5r–u), we found that the biases in the preferred motion axis and direction distributions of the thalamic inputs persist in L4 neurons. The horizontal motion axis, which dominates the AS thalamic inputs, also features prominently in the AS L4 neurons (Fig. 5v). Although a much more diverse set of directions are preferred by DS L4 neurons, the posterior-to-anterior motion direction strongly favored by the DS thalamic inputs is still represented prominently (Fig. 5w). These observations suggest that the OS/DS thalamic inputs contribute to the tuning in L4 neurons. At the same time, evidence also exists for *de novo* generation of orientation- and direction-selectivities. Although the anteroinferior-posterosuperior motion axis (green arrows in Fig. 5n,v) is preferred by few thalamic boutons, it is represented more prominently in the motion-axis distribution of AS L4 neurons (Fig. 5v). Many L4 neurons select for motion directions that are absent from the inputs (Fig. 5w).

Orientation and direction tuning of L2/3 neurons in V1

In the canonical cortical circuit, the major projection of L4 neurons is to L2/3 neurons. We observed that the OS population of L2/3 excitatory neurons are slightly more tuned (median gOSI = 0.58, median OSI = 0.78, median FWHM = 29.2°, Fig. 4v–x) than L4 neurons. However, compared to thalamic boutons and L4 neurons, the preferred orientations of the L2/3 population are much more evenly distributed (Fig. 4u). More uniform distributions were also observed for the preferred motion axis and direction of the AS (n=656, 52% of all visually responsive neurons, DSI < 0.5 in Fig. 4y) and DS (n=401, 31% of all visually responsive neurons, DSI > 0.5 in Fig. 4y) L2/3 neurons (Fig. 5x–z,aa),, respectively (Fig. 5bb,cc), with neither the horizontal motion axis nor the posterior-to-anterior motion direction dominating the distributions. The observed sharper tuning in L2/3 means less overlap in their representations for different orientations. This feature, along with the near-uniform distribution of preferred orientations, is consistent with the hypothesis that L2/3 principal cells adopt a sparse coding strategy, where a visual stimulus of a particular orientation only elicits responses from a small subset of L2/3 neurons[29].

Orientation and direction tuning of L5 neurons in V1

We next characterized the response properties of the main cortical output layer, L5. Compared to L4 and L2/3 neurons, in addition to having a smaller percentage of OS neurons (60% vs. 83% in L4 and L2/3), L5 neurons also have substantially lower OSI and broader tuning width (median gOSI = 0.46, median OSI = 0.73, median FWHM = 35.5°), although

they are still more sharply tuned than the thalamic inputs (Fig. 4aa–cc). Compared to L2/3 neurons, we found that the preferred orientations of L5 neurons are not as evenly distributed as that of L2/3 neurons (*c.f.*, Fig. 4u,z). This trend became even more evident when the direction tuning of L5 neurons was investigated – the DS population (n=294, 18% of all visually responsive neurons, DSI > 0.5 in Fig. 4dd) strongly prefers the posterior-to-anterior directions (Fig. 5ii), the same directions that dominate the thalamic input into V1. Quantitatively, compared to L2/3 and L4, L5 neurons have their preferred motion direction distribution most similar to that of thalamic inputs (Supplementary Fig. 6). These results are consistent with the notion that there are direct synaptic connections between thalamic afferents and L5 neurons in mouse V1, in line with previous electrophysiological studies[30–36], where inputs from primary thalamic nuclei were found to drive L5 neurons of the corresponding primary sensory cortex monosynaptically. They also support the emerging view that L5 neurons integrate thalamic and intracortical inputs from the entire cortical column to generate feedforward output[29].

Discussion

Using *in vivo* two-photon imaging, we carried out comprehensive characterization of orientation and direction representations along the canonical dLGN → L4 → L2/3 → L5 pathway. Imaging is particularly powerful in this context because it enables us to interrogate the circuit on the level of individual synapses, as we demonstrated on the thalamic boutons in V1. The ability to directly monitor activities at hundreds of sites simultaneously also allowed us to measure the tuning properties of tens of thousands of thalamic boutons and thousands of cortical neurons in the input and output layers, a data-rich approach that should be generally applicable to questions of circuit computation.

It is important to consider potential limitations of the imaging approach. Because the recorded calcium transients correlate with spiking activity, but not necessarily linearly to spike rate, tuning curves are susceptible to distortions by local calcium dynamics. Where comparisons can be made, the largely consistent tuning properties between our imaging data and results obtained by electrophysiology[12, 37] (Supplementary Table 1) suggest that distortion is not consequential in our system. A small amount of distortion also should not affect the calculation of preferred orientations/directions. Another potential limitation is that, when applied at depth, optical imaging suffers from aberration and scattering[38]. Even with aberration correction, *in vivo* bouton images in L4 are noisier than those in L1 (*c.f.*, **Supplementary Videos 1,2**). Thus if a subpopulation of boutons with a particular functional characteristic (e.g., AS boutons that prefer the vertical motion axis in Fig. 5l–n) were also characterized by a considerably lower fluorescence brightness than the rest of the population, the population distributions of the response properties would be skewed by the increasing difficulty in detecting these dim features at depth. We compared the average brightness of boutons within the same depth range, and found that, across all depths, there was no significant brightness difference for boutons preferring different motion axes and/or directions (Supplementary Fig. 7). Therefore, the striking orientation/direction anisotropies observed in thalamic boutons indeed reflect the biases of the tuned thalamic inputs into V1.

dLGN is the only thalamic nucleus known to project to L4 of V1. To characterize its projections into V1, we aimed to transfect as many dLGN neurons as possible, which sometimes led to spill-over expression of GCaMP6s in nearby thalamic nuclei. The only other visual thalamic nucleus that also projects to V1 is the lateral posterior thalamic nucleus (LP), whose projections are confined to L1 of V1[39]. We investigated whether the measured tuning properties of thalamic boutons in V1 are affected by GCaMP6s expression levels in LP and found little variation in orientation tuning in either L1 or L4 of mice with different amounts of LP expression (Supplementary Fig. 8). This suggests that the thalamic inputs that we characterized primarily originate from dLGN.

We describe here the first *in vivo* imaging study, to the best of our knowledge, of axons in L4 of any cortical area. Although previous studies found varying degrees of orientation tuning in mouse dLGN (~10–50%−[12] of all responsive neurons), because these experiments only measured the tuning properties of neurons in dLGN, rather than their projections in V1, whether the tuned information is sent to the main thalamorecipient L4 in V1 remained an outstanding question. Using retrograde tracing and anatomical hypotheses, a recent study suggested that the tuned pathway is confined to the superficial layers of the cortex, representing a circuit that is segregated from the geniculocortical pathway carrying untuned input into deeper layers[14]. This is consistent with the long-standing and dominant belief that orientation selectivity in dLGN, if indeed it exists, does not provide selectivity to the bulk of V1[15]. By direct functional characterization of thalamic boutons in L4, we reached the contrary conclusion: the tuned and non-tuned inputs are conveyed to and intermixed in all layers that we investigated, with about half of all boutons exhibiting significant orientation tuning, and half of these exhibiting direction selectivity.

Our finding that tuned inputs are conveyed to L4 of primary visual cortex suggests a refinement of mechanistic models that assume the mammalian primary visual cortex to be entirely responsible for computing these features from untuned inputs. Comparing the orientation and direction preferences of the LGN inputs and L4 excitatory neurons, we found that the dominant geniculate orientation and motion direction biases are preferred by a large fraction of L4 neurons, but there are also L4 neurons with tuning preferences that are largely absent in the thalamic input. Taken together, our results suggest that multiple mechanisms[7, 40, 41] are at work in the thalamocortical transformation of orientation- and direction-selectivity in mouse V1, where cortical tuning may be constructed from untuned thalamic inputs, directly inherited from OS/DS thalamic neurons, or result from a complex interplay of both tuned and untuned inputs[42]. The population-level analyses presented here cannot distinguish among these scenarios. To resolve how the tuned thalamic inputs contribute to the orientation tuning of individual L4 neurons, we need direct measurements of input-output relationships on the single neuron level. The first step would be to find the post-synaptic targets of these tuned axons, whereas a definitive experiment would be to measure the tuning properties of all the thalamocortical synapses of a single L4 neuron.

Given previous whole cell recording studies[5, 42], the OS/DS dLGN neurons that are highly nonlinear in their spatial summation[10, 12, 43] are unlikely to contribute directly to V1 simple cells[5, 44]. Instead, they may contribute to the cortical selectivities through alternative pathways, for example, by synapsing onto non-simple-cell population[37] or by providing the

orientation/direction biases to shape the cortical circuit during development[45]. More generally, although varying degrees of orientation- and direction-selectivity have been observed in dLGN of rabbit[43], cat[46, 47], and monkey[48], the extent to which our results will generalize across mammalian species remains largely an empirical question.

Methods

All experimental protocols were conducted according to the National Institutes of Health guidelines for animal research and were approved by the Institutional Animal Care and Use Committee at Janelia Research Campus, Howard Hughes Medical Institute. Data collection and analysis were not performed blind to the conditions of the experiments. A supplementary methods checklist is available.

Mice

Wild-type male mice were used for *in vivo* functional imaging of visual thalamic axons (older than P60, C57BL/6J). *Scnn1a*-Tg3-Cre mice (Jax no. 009613), *Thy1*-GCaMP6 GP4.3 mice, and *Rbp4*-Cre mice (MMRRC no. 031125-UCD) of both sexes (older than P60) were used for *in vivo* functional imaging of L4, L2/3, and L5 neurons, respectively. Male and *Scnn1a*-Tg3-Cre mice were used in the histology experiment. Sample sizes (number of mice, cells, and/or boutons) for each experiment are stated in main text.

Virus injections

Mice were anaesthetized with isoflurane (1–2% by volume in O_2) and given the analgesic buprenorphine (SC, 0.3 mg/kg). Virus injection was performed using a glass pipette beveled at 45° with a 15–20 μm opening and back-filled with mineral oil. A fitted plunger controlled by a hydraulic manipulator (Narashige, MO10) was inserted into the pipette and used to load and inject the viral solution. To prevent virus leakage before reaching the injection site, the tip of glass pipette was filled with ~1 nl saline right before injection. To prevent backflow during withdrawal, the pipette was kept in the brain for over 10 min and then the plunger was withdrawn (~1 nl in volume) before the pipette was pulled up.

To demonstrate the projection pattern of visual thalamic axons in V1, 20 nl of AAV2/1.CAG.FLEX.tdTomato.WPRE.bGH-containing solution (~7×10^{12} infectious units per ml) was injected into V1 of Scnn-Tg3-Cre mice to label L4 neurons (left hemisphere, 3.4 mm posterior to Bregma; 2.7 mm lateral from midline; 0.3 mm below pia), and 20 nl of AAV2/1.hSynapsin.EGFP.WPRE.bGH-containing solution (~3×10^{13} infectious units per ml) was injected into dLGN (left hemisphere, 2.1mm posterior to Bregma; 2.3mm lateral from midline; 2.5 mm below pia).

For calcium imaging with GCaMP6s, 20~30 nl of AAV2/1-syn-GCaMP6s-WPRE-SV40-containing solution (~2×10^{13} infectious units per ml) was slowly injected into dLGN for axon imaging, and 20 nl of AAV1-syn-flex-GCaMP6s-WPRE-SV40-containing solution (~2.4×10^{13} infectious units per ml) was injected per injection site into V1 for cortical L4 (*Scnn1a*-Tg3-Cre mice: 3 injection sites in left hemisphere centered at 3.4 mm posterior to Bregma; 2.7 mm lateral from midline; 0.3 mm below pia. Injection sites are ~250 μm apart) or cortical L5 (*Rbp4*-Cre mice: 0.4 mm below pia) neuron imaging[20].

Although the injection sites in the visual thalamus were always within dLGN, there were sometimes spill-over expressions in neighboring ventral LGN (vLGN), intergeniculate leaflet (IGL), and lateral posterior thalamic nucleus (LP). vLGN and IGL do not project to V1[49]; compared to dLGN, projections from LP to V1 are much sparser and limited to L1[39, 50]. Therefore, the vast majority of the thalamic axons we observed in V1 originated from dLGN.

Cranial window implant

Craniotomy was carried out at the same time of virus injection for calcium imaging experiments. Using aseptic technique, a 2.5 mm diameter craniotomy was made over the left primary visual cortex (V1) (center: 3.4 mm posterior to Bregma; 2.7 mm lateral from midline) of the anaesthetized mice. Dura was left intact. 2 μl of red fluorescent bead solution (2-μm diameter; 1:500 in saline; Life Technologies, F-8826) was deposited on dura surface for correcting aberration induced by both cranial window and microscope. A glass window made of either a single coverslip (Fisher Scientific no. 1.5) or two coverslips bonded with ultraviolet cured optical adhesives (Norland Optical Adhesives 61) was embedded in the craniotomy and sealed in place with dental acrylic. A titanium head-post was attached to the skull with cyanoacrylate glue and dental acrylic[20].

Visual stimulation

Visual stimuli were presented by back projection on a screen made of Teflon® film using a custom-modified DLP® projector. The screen was positioned 17 cm from the right eye, covering 75° × 75° degrees of visual space and oriented at ~40° to the long axis of the animal. The projector was modified to provide equilength and linear frames at 360 Hz (designed by Anthony Leonardo, Janelia Research Campus, Howard Hughes Medical Institute, and Lightspeed Design Inc, model WXGA-360). Its lamp housing was replaced by a holder for liquid light guide, through which visible light (450–495 nm) generated by a LED light source (SugarCUBE) was delivered to the screen. The maximal luminance measured at the location of animal eyes was 437 nW/mm^2.

Visual stimuli were generated using custom-written codes. To measure orientation-tuning, full-field square gratings were presented in 8 (for boutons, L4, and L5 neurons) or 12 (for L2/3 neurons) directions in a pseudorandom sequence for 12 sec each, during which time each stimulus was static for the first and last 3 sec and moving during the middle 6 sec. Gratings had 100% contrast, 0.07 cyc/deg, and drifted at 26 deg/sec (i.e., a temporal frequency of ~2 Hz). A total of 10 trials were presented in each measurement.

Two-photon imaging

Imaging was performed with an adaptive-optical two-photon fluorescence microscope[51] 2–4 weeks after virus injection, when most neurons in dLGN and cortex exhibited cytosolic-only expression[52] of GCaMP6s (Fig. 1b, Fig. 3). Mice were head-fixed and awake during the imaging period. To habituate the mice to experimental handling, 1 week after surgery, each mouse was head-fixed onto the sample stage with its body restrained under a half-cylindrical cover, which reduces struggling and prevents substantial body movements such as running. The habituation procedure was repeated 3–4 times for each animal, and each time for 15–60

mins. Each experiment session lasted between 45 minutes to 3 hours. Multiple sections (imaging planes) may be imaged within the same mouse. GCaMP6s was excited at 900 nm with a Ti:Sapphire laser (Ultra II, Coherent) that was focused by either a Nikon 16×, 0.8 NA or an Olympus 25×, 1.05 NA objective. Emitted fluorescence photons reflected off a dichroic long-pass beamsplitter (FF665-Di02-25×36; Semrock) and were detected by a photomultiplier tube (H7422PA-40, Hamamatsu).

Images of axons were acquired from the brain surface down to 400 μm below pia using home-made LabVIEW software. Laser power measured post objective varied between 20 and 175 mW, with higher power used at deeper depth. Out of 28 image sections for boutons 300–400 μm below pia, three image sections were taken with 175 mW; one image section were taken with 156 mW; while all others were taken at power less than 140 mW. Typical time for mapping the orientation selectivity of a single image section is ~15 minutes. We did not observe photobleaching or photodamage, even when we imaged a single plane at 350 μm depth with 156 mW post-objective power for 45 minutes (e.g., ROI6, Supplementary Fig. 3d). Images of L4, L2/3, and L5 neurons were taken at 280–410 μm, 60–280 μm, and 410–540 μm below pia, respectively, at post-objective power of 20 to 90 mW. Imaging areas for both axons and neurons are within 3.4±0.6 mm posterior to Bregma and 2.7±0.6 mm lateral from midline. Typical images had 300 × 300 pixels, at 0.3–0.35 μm per pixel and ~2 Hz frame rate for axons, and 1–1.6 μm per pixel and 3–4 Hz frame rate for cell bodies. The optical aberration introduced by the cranial window and microscope was corrected following previously described adaptive optical procedure[23] using red fluorescent beads deposited between the cranial window and the brain.

Brain histology and confocal imaging

To validate the injection site, after each calcium imaging experiment, Cholera Toxin Subunit B (CTB) conjugated with Alexa-594 (1 μg in 2 μl saline) was injected into right eye of the mouse to allow anterograde labeling of retinal ganglion cell axons in visual thalamus. 24–48 hours later, mice were deeply anaesthetized with isoflurane and transcardially perfused with PBS and then 4% PFA. Brains were removed and post fixed overnight in PFA. Coronal brain slices were cut to 100 μm thickness using a Leica microtome (V1200S, Leica).

To retrogradely label the neurons projecting to V1, ~100 nl of Fluoro-Gold™ (5% diluted in distilled water) was injected into V1. One week later, the brain was harvested and coronal brain slices were cut to 100 μm thickness. All brain slices were mounted in Vector Shield mounting solution.

Fluorescence images of these sectioned brains were acquired on a laser scanning confocal microscope (Zeiss LSM 710) equipped with 405, 488, and 561nm excitation lasers. Images were collected using the following Plan-Apochromat objectives: 10×/0.45 NA (optical section step of 2 μm), 20×/0.8 NA (optical section step of 1.0 μm), 40×/1.3 NA oil immersion (optical section step of 0.5μm), and 63×/1.4 NA oil immersion (optical section step of 0.5μm).

Image processing and analysis

The time-lapse calcium imaging stacks were analyzed with custom programs written in MATLAB (Mathworks). Lateral motion present in head-fixed awake mice was corrected using a cross-correlation-based registration algorithm[18], where cross-correlation was calculated to determine frame shift in x and y directions. Because of the extremely low signal of GCaMP6s sans activity (Supplementary Fig. 3a), the mean projection of the whole stack was used as the registration reference. Iterating this registration procedure led to the continuous decrease of $\sum_k (\Delta x_k^2 + \Delta y_k^2)$, where Δx_k and Δy_k represent the horizontal and vertical shifts of frame k relative to the reference image, respectively. Typically, 7 iterations were sufficient for axon data (Supplementary Fig. 3b).

Cortical neurons were outlined by hand as regions of interest (ROIs). To identify potential boutons, we used the mean projection of the registered stack, and outlined varicosities of 1–3 μm in diameter (Supplementary Fig. 3c). We then calculated the fluorescence time courses of the ROIs. For each ROI, we used the mode from the fluorescence intensity histogram as the baseline fluorescence F_0, and calculate its calcium transient as $\Delta F/F(\%) = (F - F_0) / F_0 \times 100$ (Supplementary Fig. 3d). The final calcium transient to each visual stimulus (e.g., Fig. 1j–l) was the average of ten trials. A ROI was considered responsive if its maximal $\Delta F/F$ during the presentation of visual stimuli was above 10%. Of 33,263 boutons outlined from 21 wild-type mice, 27,902 (84%) were visually responsive; Of 1,511 L4 neurons outlined from 3 *Scnn1a*-Tg3-Cre mice, 1,239 (82%) were visually responsive; Of 2,608 L2/3 neurons outlined from 6 *Thy1*-GCaMP6 GP4.3 mice, 1,279 (49%) were visually responsive; Of 1,677 L5 neurons outlined from 5 *Rbp4*-Cre mice, 1,554 (93%) were visually responsive. No statistical methods were used to predetermine sample sizes, but our sample sizes are similar to or larger than those generally employed in the field.

Tuning Curve Analysis

The response R of each ROI to a visual stimulus was defined as the average $\Delta F/F$ across the 6-second window of drifting gratings. The distribution of R was assumed to be normal and variances were assumed to be equal across grating angle θ but this was not formally tested. For ROIs with significantly different responses across the drifting directions (one-sided ANOVA, $P < 0.05$), we fit their normalized response tuning curves to grating drifting angle θ (e.g., Fig. 1m–o) with a bimodal Gaussian function[22]:

$$R(\theta) = R_{\text{offset}} + R_{\text{pref}} e^{-\frac{\text{ang}(\theta - \theta_{\text{pref}})^2}{2\sigma^2}} + R_{\text{oppo}} e^{-\frac{\text{ang}(\theta - \theta_{\text{pref}} + 180)^2}{2\sigma^2}}.$$

Here θ_{pref} is the preferred orientation, R_{offset} is a constant offset, and R_{pref} and R_{oppo} are the responses at θ_{pref} and $\theta_{\text{pref}}-180$ degree, respectively. $\text{ang}(x) = \min(x, x-360, x+360)$ wraps angular difference values onto the interval 0° to 180°. The tuning width for the preferred orientation is calculated as the full width at half maximum (FWHM) of the Gaussian function, $2\sqrt{2\ln 2}\sigma$.

To determine the goodness of fit, we calculated the fitting error E as well as the coefficient of determination $\Re^2$:

$$E=\sum_{\theta}(R_{\text{measured}}(\theta)-R_{\text{fitted}}(\theta))^2,$$

$$\Re^2=1-\frac{\sum_{\theta}(R_{\text{measured}}(\theta)-R_{\text{fitted}}(\theta))^2}{\frac{n-1}{n}\sum_{\theta}(R_{\text{measured}}(\theta)-\overline{R})^2}$$

where $R_{\text{measured}}(\theta)$ and $R_{\text{fitted}}(\theta)$ are the measured and fitted responses at θ, respectively. $\overline{R}$ is the mean of $R_{\text{measured}}(\theta)$. Only ROIs with $E < 0.4$ and $\Re^2 > 0.6$ were defined as orientation-selective (OS). Applying a more stringent definition, with $E < 0.2$ and $\Re^2 > 0.8$, reduced the number of OS units but did not affect the conclusions of this work. Image registration and tuning curve analysis routines are available upon request.

Supplementary Material

Refer to Web version on PubMed Central for supplementary material.

Acknowledgements

We thank M. Cembrowski, Y. Dan, R. Egnor, A. Kerlin, J. Magee, G. Murphy, S. Sternson, M. Stryker, and K. Svoboda for comments on the manuscript; A. Hu for help with histology. This work was supported by Howard Hughes Medical Institute.

References

1. Douglas RJ, Martin KAC. Neuronal circuits of the neocortex. Ann. Rev. Neurosci. 2004; 27:419–451. [PubMed: 15217339]
2. Hubel DH, Wiesel TN. Receptive fields of single neurones in the cat's striate cortex. J. Physiol. 1959; 148:574–591. [PubMed: 14403679]
3. Sherman SM. Thalamocortical interactions. Curr. Opin. Neurobio. 2012; 22:575–579.
4. Reid RC, Alonso J-M. Specificity of monosynaptic connections from thalamus to visual cortex. Nature. 1995; 378:281–284. [PubMed: 7477347]
5. Lien AD, Scanziani M. Tuned thalamic excitation is amplified by visual cortical circuits. Nature Neurosci. 2013; 16:1315–1323. [PubMed: 23933748]
6. Li Y-T, Ibrahim LA, Liu B-H, Zhang LI, Tao HW. Linear transformation of thalamocortical input by intracortical excitation. Nature Neurosci. 2013; 16:1324–1330. [PubMed: 23933750]
7. Hubel DH, Wiesel TN. Receptive fields, binocular interaction and functional architecture in the cat's visual cortex. J. Physiol. 1962; 160:106–154. [PubMed: 14449617]
8. Chapman B, Zahs K, Stryker M. Relation of cortical cell orientation selectivity to alignment of receptive fields of the geniculocortical afferents that arborize within a single orientation column in ferret visual cortex. J. Neurosci. 1991; 11:1347–1358. [PubMed: 2027051]
9. Marshel, James H.; Kaye, Alfred P.; Nauhaus, I.; Callaway, Edward M. Anterior-posterior direction opponency in the superficial mouse lateral geniculate nucleus. Neuron. 2012; 76:713–720. [PubMed: 23177957]
10. Piscopo DM, El-Danaf RN, Huberman AD, Niell CM. Diverse visual features encoded in mouse lateral geniculate nucleus. J. Neurosci. 2013; 33:4642–4656. [PubMed: 23486939]
11. Scholl B, Tan AYY, Corey J, Priebe NJ. Emergence of orientation selectivity in the mammalian visual pathway. J. Neurosci. 2013; 33:10616–10624. [PubMed: 23804085]
12. Zhao X, Chen H, Liu X, Cang J. Orientation-selective responses in the mouse lateral geniculate nucleus. J. Neurosci. 2013; 33:12751–12763. [PubMed: 23904611]

13. Vaney DI, Sivyer B, Taylor WR. Direction selectivity in the retina: symmetry and asymmetry in structure and function. Nat. Rev. Neurosci. 2012; 13:194–208. [PubMed: 22314444]
14. Cruz-Martin A, et al. A dedicated circuit links direction-selective retinal ganglion cells to the primary visual cortex. Nature. 2014; 507:358–361. [PubMed: 24572358]
15. Niell C. Cell types, circuits, and receptive fields in the mouse visual cortex. Annu. Rev. Neurosci. 2015; 38:413–431. [PubMed: 25938727]
16. Chen T-W, et al. Ultrasensitive fluorescent proteins for imaging neuronal activity. Nature. 2013; 499:295–300. [PubMed: 23868258]
17. Antonini A, Fagiolini M, Stryker MP. Anatomical correlates of functional plasticity in mouse visual cortex. J. Neurosci. 1999; 19:4388–4406. [PubMed: 10341241]
18. Guizar-Sicairos M, Thurman ST, Fienup JR. Efficient subpixel image registration algorithms. Opt Lett. 2008; 33:156–158. [PubMed: 18197224]
19. De Paola V, et al. Cell type-specific structural plasticity of axonal branches and boutons in the adult neocortex. Neuron. 2006; 49:861–875. [PubMed: 16543134]
20. Petreanu L, et al. Activity in motor-sensory projections reveals distributed coding in somatosensation. Nature. 2012; 489:299–303. [PubMed: 22922646]
21. Glickfeld LL, Andermann ML, Bonin V, Reid RC. Cortico-cortical projections in mouse visual cortex are functionally target specific. Nature Neurosci. 2013; 16:219–226. [PubMed: 23292681]
22. Carandini M, Ferster D. Membrane potential and firing rate in cat primary visual cortex. J. Neurosci. 2000; 20:470–484. [PubMed: 10627623]
23. Ji N, Sato TR, Betzig E. Characterization and adaptive optical correction of aberrations during in vivo imaging in the mouse cortex. Proc. Nat. Acad. Sci. 2011
24. Wang C, et al. Multiplexed aberration measurement for deep tissue imaging in vivo. Nature Meth. 2014; 11:1037–1040.
25. Wang K, et al. Direct wavefront sensing for high-resolution in vivo imaging in scattering tissue. Nature Comm. 2015; 6
26. Madisen L, et al. A robust and high-throughput Cre reporting and characterization system for the whole mouse brain. Nature Neurosci. 2010; 13:133–140. [PubMed: 20023653]
27. Dana H, et al. *Thy1*-GCaMP6 transgenic mice for neuronal population imaging *in vivo* . PLoS ONE. 2014; 9:e108697. [PubMed: 25250714]
28. Ringach DL, Shapley RM, Hawken MJ. Orientation selectivity in macaque V1: diversity and laminar dependence. J. Neurosci. 2002; 22:5639–5651. [PubMed: 12097515]
29. Harris KD, Mrsic-Flogel TD. Cortical connectivity and sensory coding. Nature. 2013; 503:51–58. [PubMed: 24201278]
30. Bullier J, Henry GH. Laminar distribution of first-order neurons and afferent terminals in cat striate cortex. J. Neurophysiol. 1979; 42:1271–1281. [PubMed: 490198]
31. Martin KA, Whitteridge D. Form, function and intracortical projections of spiny neurones in the striate visual cortex of the cat. J. Physiol. 1984; 353:463–504. [PubMed: 6481629]
32. Armstrong-James M, Fox K, Das-Gupta A. Flow of excitation within rat barrel cortex on striking a single vibrissa. J. Neurophysiol. 1992; 68:1345–1358. [PubMed: 1432088]
33. de Kock CPJ, Bruno RM, Spors H, Sakmann B. Layer- and cell-type-specific suprathreshold stimulus representation in rat primary somatosensory cortex. J. Physiol. 2007; 581:139–154. [PubMed: 17317752]
34. Constantinople CM, Bruno RM. Deep cortical layers are activated directly by thalamus. Science. 2013; 340:1591–1594. [PubMed: 23812718]
35. Sun YJ, Kim Y-J, Ibrahim LA, Tao HW, Zhang LI. Synaptic mechanisms underlying functional dichotomy between intrinsic-bursting and regular-spiking neurons in auditory cortical layer 5. J. Neurosci. 2013; 33:5326–5339. [PubMed: 23516297]
36. Petreanu L, Mao T, Sternson SM, Svoboda K. The subcellular organization of neocortical excitatory connections. Nature. 2009; 457:1142–1145. [PubMed: 19151697]
37. Niell CM, Stryker MP. Highly selective receptive fields in mouse visual cortex. J. Neurosci. 2008; 28:7520–7536. [PubMed: 18650330]

38. Ji N. The practical and fundamental limits of optical imaging in mammalian brains. Neuron. 2014; 83:1242–1245. [PubMed: 25233304]
39. Oh SW, et al. A mesoscale connectome of the mouse brain. Nature. 2014; 508:207–214. [PubMed: 24695228]
40. Kuhlmann L, Vidyasagar TR. A computational study of how orientation bias in the lateral geniculate nucleus can give rise to orientation selectivity in primary visual cortex. Front. Sys. Neurosci. 2011; 5 Article 81.
41. Priebe, Nicholas J.; Ferster, D. Mechanisms of neuronal computation in mammalian visual cortex. Neuron. 2012; 75:194–208. [PubMed: 22841306]
42. Miller LM, Escabí MA, Read HL, Schreiner CE. Functional convergence of response properties in the auditory thalamocortical system. Neuron. 2001; 32:151–160. [PubMed: 11604146]
43. Hei X, et al. Directional selective neurons in the awake LGN: response properties and modulation by brain state. J. Neurophysiol. 2014; 112:362–373. [PubMed: 24790175]
44. Li Y-T, Liu B-H, Chou X-L, Zhang LI, Tao HW. Strengthening of direction selectivity by broadly tuned and spatiotemporally slightly offset inhibition in mouse visual cortex. Cerebral Cortex. 2014
45. Rochefort NL, et al. Development of direction selectivity in mouse cortical neurons. Neuron. 2011; 71:425–432. [PubMed: 21835340]
46. Vidyasagar TR, Urbas JV. Orientation sensitivity of cat LGN neurones with and without inputs from visual cortical areas 17 and 18. Exp. Brain Res. 1982; 46:157–169. [PubMed: 7095028]
47. Vidyasagar TR, Jayakumar J, Lloyd E, Levichkina EV. Subcortical orientation biases explain orientation selectivity of visual cortical cells. Physiol. Rep. 2015; 3:e12374. [PubMed: 25855249]
48. Smith EL, Chino YM, Ridder WH, Kitagawa K, Langston A. Orientation bias of neurons in the lateral geniculate nucleus of macaque monkeys. Vis. Neurosci. 1990; 5:525–545. [PubMed: 2085469]
49. Harrington ME. The ventral lateral geniculate nucleus and the intergeniculate leaflet: interrelated structures in the visual and circadian systems. Neurosci. Biobehav. Rev. 1997; 21:705–727. [PubMed: 9353800]
50. Sanderson KJ, Dreher B, Gayer N. Prosencephalic connections of striate and extrastriate areas of rat visual cortex. Exp. Brain Res. 1991; 85:324–334. [PubMed: 1716594]
51. Ji N, Milkie DE, Betzig E. Adaptive optics via pupil segmentation for high-resolution imaging in biological tissues. Nature Meth. 2010; 7:141–147.
52. Tian L, et al. Imaging neural activity in worms, flies and mice with improved GCaMP calcium indicators. Nature Meth. 2009; 6:875–881.

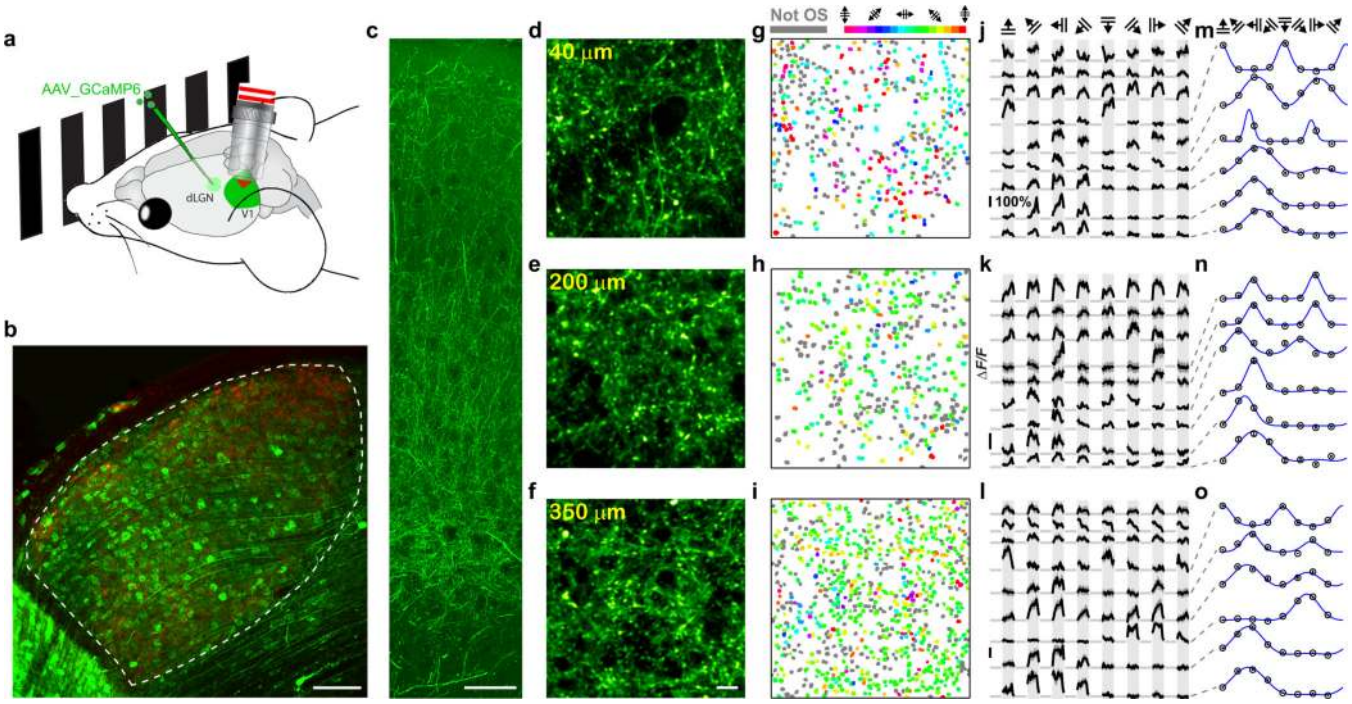

Fig. 1. *In vivo* calcium imaging of thalamic axons in V1

(**a**) *In vivo* imaging of GCaMP6s$^+$ thalamic axons in V1 of head-fixed awake mouse. (**b**) GCaMP6s$^+$ neurons (green) in dLGN outlined by retinal ganglion cell axons (red). Scale bar: 100 μm. (**c**) GCaMP6s$^+$ axons in V1. Scale bars: 50 μm. (**d–f**) *In vivo* images of GCaMP6s$^+$ thalamic axons at (**d**) 40 μm, (**e**) 200 μm, and (**f**) 350 μm below pia in V1. Scale bar: 10 μm. (**g–i**) Varicosities (putative boutons) from **d–f** color-coded by their preferred orientation. Gray, boutons with visual response but no orientation selectivity (OS). (**j–l**) Example Δ*F/F* calcium transients (10 trial average) for boutons from **d–f**. (**m–o**) Tuning curves for the bottom six boutons in **j–l**. Dark gray shadow (**j–l**) and error bars (**m–o**): s.e.m.. Representative images from 21 mice.

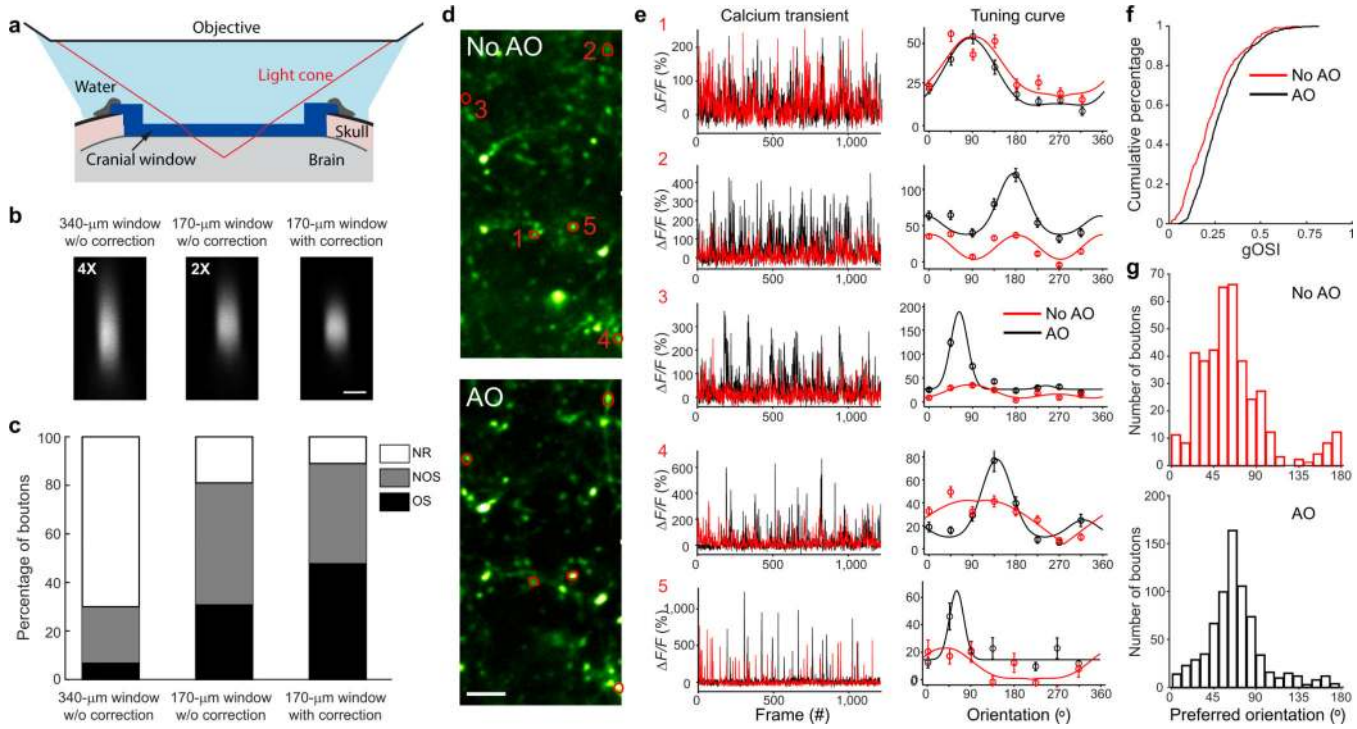

Figure 2. Adaptive optics is essential for tuning curve characterization

(**a**) Excitation light aberrated by refractive index differences between water and cranial window/brain. (**b**) Axial images of a 2-μm bead below a 340-μm window, a 170-μm window, and a 170-μm window with adaptive optics (AO) correction. Images taken without AO have 4× and 2× gain for better visibility. Scale bar: 2 μm. (**c**) Percentages of non-responsive (NR), not OS (NOS), and OS boutons at 300–350 μm depth under the conditions in **b**. (**d**) Images of GCaMP6s+ axons at 170 μm depth measured without and with AO. Images are saturated to improve visibility of dim features. Scale bar: 10 μm. (**e**) Calcium transients and tuning curves for ROIs labeled in **d** measured without (red) and with (black) AO. Error bars: s.e.m.. (**f**) Cumulative distributions of global orientation-selectivity index (gOSI) for boutons at 300–350 μm depth measured without and with AO. (**g**) Their preferred orientation distributions measured without and with AO. **d–g**, cranial window thickness: 170 μm. **f,g**, same data as in **c**, boutons imaged under 170-μm window without and with AO correction and analyzed with independent ROI selections.

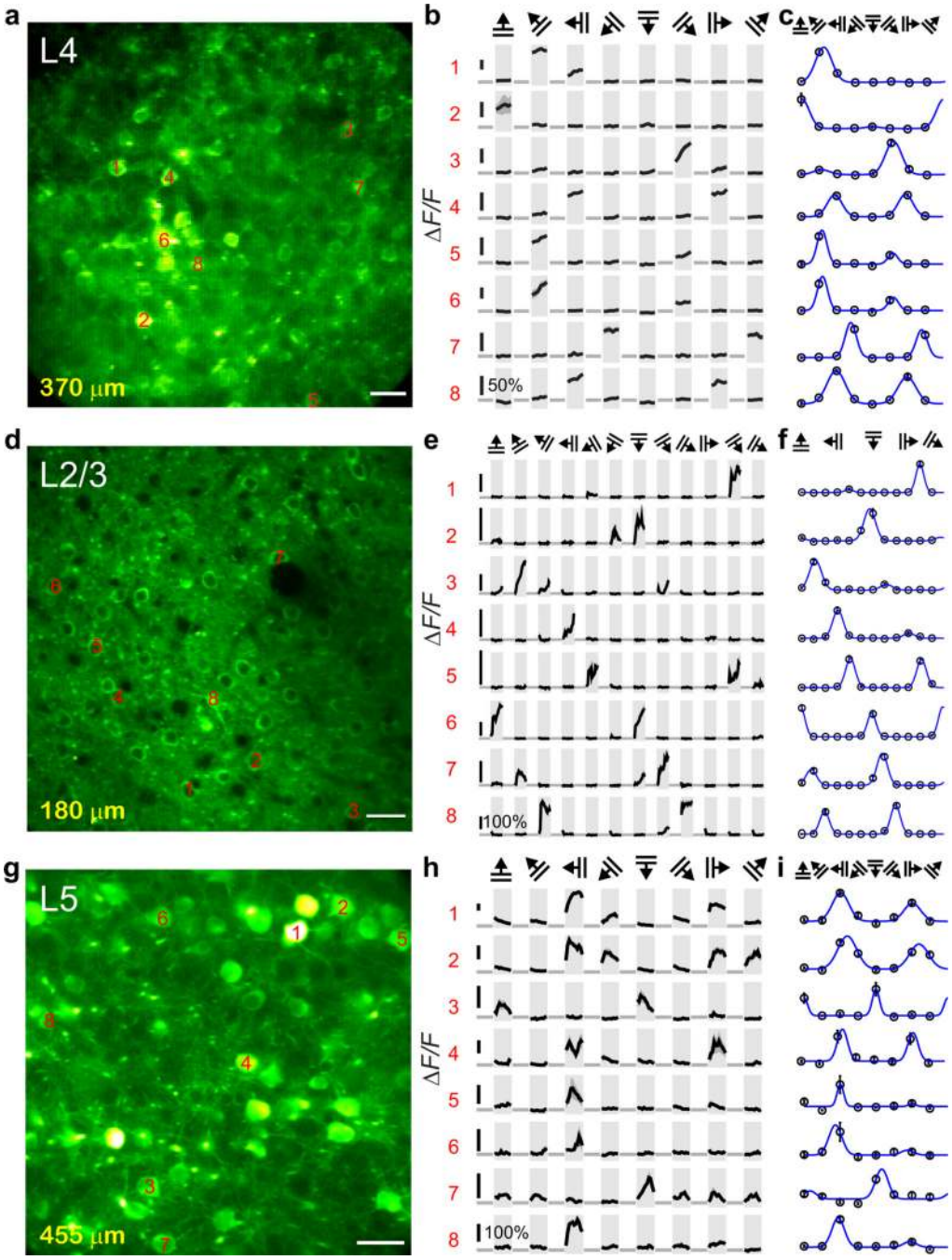

Fig. 3. Characterization of tuning properties of L4, L2/3, and L5 neurons in V1

(**a**) An example *in vivo* image of L4 neurons. Numbers label example somata. (**b**) Calcium transients Δ*F/F*, and (**c**) tuning curves of the somata in **a**; Light gray background in **b**: 6-sec drifting grating (topmost labels) presentation; Dark gray shade in **b** and error bars in **c**: s.e.m.. (**d–i**) Example *in vivo* images, calcium transients, and tuning curves of (**d–f**) L2/3 and (**g–i**) L5 neurons. Scale bar: 25 μm. Representative results from 3 *Scnn1a*-Tg3-Cre (L4), 6 *Thy1*-GCaMP6 GP4.3 (L2/3), and 5 *Rbp4*-Cre (L5) mice.

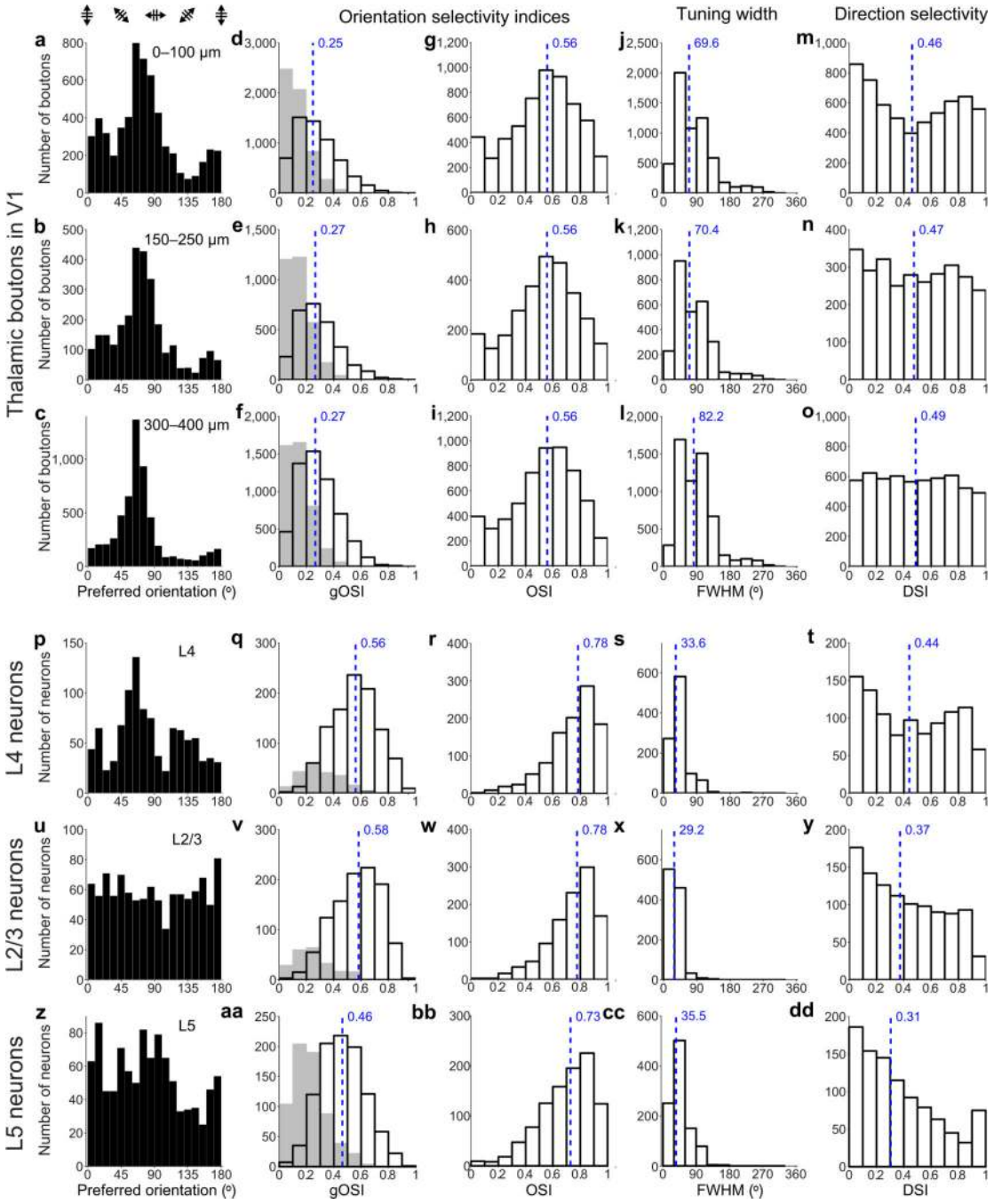

Fig. 4. Orientation tuning of thalamic boutons and neurons in V1

(**a–o**) Orientation tuning of thalamic boutons: histogram distributions of (**a–c**) preferred orientation, (**d–f**) global orientation-selective index (gOSI), (**g–i**) orientation-selective index (OSI), (**j–l**) tuning width (FWHM), (**m–o**) direction-selective index (DSI) for OS boutons 0–100 µm, 150–250 µm, and 300–400 µm below pia. (**p–dd**) Orientation tuning properties of cortical neurons: distributions of preferred orientation, gOSI, OSI, FWHM, and DSI for (**p–t**) L4, (**u–y**) L2/3, and (**z–dd**) L5 neurons. Gray histograms in **d–f,q,v,aa**: gOSI distributions for non-OS units. Blue dashed lines: distribution medians.

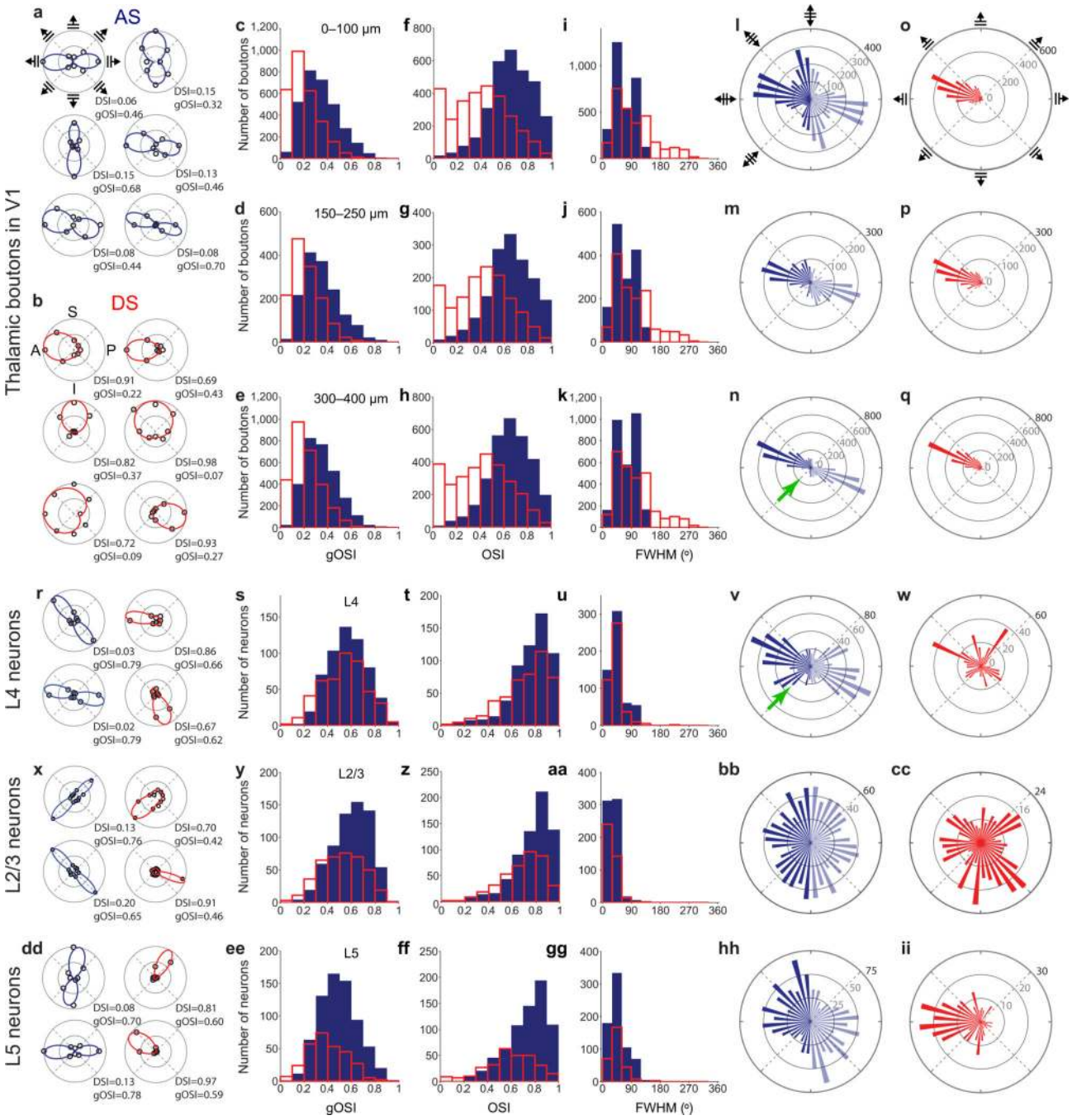

Fig. 5. Direction tuning of thalamic boutons and neurons in V1

(**a–q**) Direction tuning of thalamic boutons: Example polar-plot tuning curves of (**a**) axis-selective (AS) and (**b**) direction-selective (DS) boutons; A, P, S, I in **b**: anterior, posterior, superior, and inferior directions; Bottom right: DSI & gOSI. (**c–e**) gOSI, (**f–h**) OSI, and (**i–k**) tuning curve FWHM distributions for AS (blue) and DS (red) boutons 0–100 µm, 150–250 µm, and 300–400 µm below pia; (**l–n**) Circular histograms of preferred motion axis for AS units (bar orientation: preferred motion axis; bar length: # of units); Bars reflected for displaying axis selectivity (faded and full-color bars represent the same data); (**o–q**) Circular

histograms of preferred motion direction for DS units (bar direction: motion direction). (**r–ii**) Direction tuning of cortical neurons: Example tuning curves, distributions of gOSI, OSI, FWHM, preferred motion axis for AS, and preferred motion direction for DS (**r–w**) L4, (**x–cc**) L2/3, and (**dd–ii**) L5 neurons. Green arrows indicate the anteroinferior-posterosuperior motion axis.